

Coherent Remote Control over Nano-Emitters Embedded in Polymer Waveguides

Alexander Landowski,^{1,*} Jonas Gutsche,¹ Stefan Guckenbiehl,¹
Marius Schönberg,¹ Georg von Freymann,^{1,2} and Artur Widera^{1,3}

¹*Department of Physics and State Research Center OPTIMAS,
University of Kaiserslautern, Erwin-Schrodinger-Str. 46, 67663 Kaiserslautern, Germany*

²*Fraunhofer Institute for Industrial Mathematics ITWM,
Fraunhofer-Platz 1, 67663 Kaiserslautern, Germany*

³*Graduate School Materials Science in Mainz, Erwin-Schrodinger-Str. 46, 67663 Kaiserslautern, Germany*

We report the integration of individual, singlecrystalline nanodiamonds containing many nitrogen-vacancy centers (NV) into three-dimensional direct-laser-written waveguides. We excite the NV center by light propagating through the waveguide, and we show that emitted fluorescence can be efficiently coupled to the waveguide modes. While the autofluorescence of the waveguides is much smaller than the fluorescence of the NV ensembles, time-decay of the fluorescence after pulsed excitation allows for highly selective separation of the NV fluorescence. Moreover, we investigate optically detected magnetic resonance spectra as well as Rabi nutations recorded through the waveguide coupled signal. Our work shows that the system is ideally suited for magnetometry and remote read-out of spin coherence in a freely configurable waveguide network, overcoming the need for direct optical access of NV centers in nanodiamonds.

I. INTRODUCTION

Nitrogen-vacancy (NV) centers in diamond have advanced to a highly promising nano-scale probe. A prominent feature of the NV is optical initialization and read-out of its spin degree of freedom [1]. Because of coherence times up to $T_2 = 3$ ms at room temperature [2] and its high sensitivity to external fields, it is widely used to detect DC and AC magnetic fields [3–6], to sense temperature distributions in biological samples [7], and even to show a loophole free test of the bell inequality [8].

Most such applications require direct optical access to the NV center usually using microscopes with high numerical apertures. An alternative way to guide the NV center's signal to a detector are waveguides. Such waveguides, directly fabricated from a diamond membrane [9–12] or micrometer long, free standing polymer waveguides [13, 14], guiding NV fluorescence signal have been reported elsewhere. Moreover, it has been shown that waveguides as well as NV centers can be deterministically defined inside bulk diamond using a direct laser writing technique [15].

Here, we show the integration of individual singlecrystalline nanodiamonds containing an ensemble of NV centers into a flexible, three-dimensional waveguide networks that can be on millimeter length scales. The waveguides allow remote excitation as well as detection of the NV centers' fluorescence, relaxing the need for direct optical access to the nanodiamond. The waveguides can be configured to feature extended planar networks lying on the substrate with three-dimensional features, *e.g.*, for perpendicular coupling. We harness the optical waveguide both to address and to bidirectionally detect the NV center ensemble. For addressing, a green laser beam for optical initialization and read-out of the spin ensemble

is fed through the waveguide to the nanodiamond. For detection, the fraction of total fluorescence, which is coupled to the waveguide, is guided to the microscope's focal plane, where input and output ports of the waveguide are imaged simultaneously [16]. Since the waveguides may have three-dimensional features, NV center ensembles lying in different focal planes can be addressed simultaneously without sample translation, while keeping one side of the sample accessible for additional manipulation. Further, the integration of NV centers into a waveguide might enhance the applicability of these color centers as probes in biology. Since the excitation light is guided inside the waveguide, its phototoxicity is strongly reduced in contrast to confocal microscopy, where the excitation light is focused through the sample volume. This paves the way to build three dimensional arrays of sensors, detecting the amplitude and direction of, *e.g.*, magnetic fields on micrometer scales, even for very sensitive samples, while keeping optical access to the sample from both sides.

II. EXPERIMENTAL SYSTEM

The NV center is a paramagnetic point defect in the diamond lattice, see 1 (a),(b). Its structure, shown in the inset of FIG. 1 (b) is composed of a substitutional nitrogen atom (N) and an adjacent vacant lattice site (V). We use the negatively charged state, which binds an additional electron from nearby N donors [20]. Its ground state is a spin triplet with 2.87 GHz zero field splitting between the $m_s = 0$ and degenerate $m_s = \pm 1$ spin states, quantized along the NV-axis. This degeneracy is lifted in presence of an external magnetic field. Ground-state splitting and Zeeman shift, caused by the magnetic field component along the NV-axis, can be described by [20]

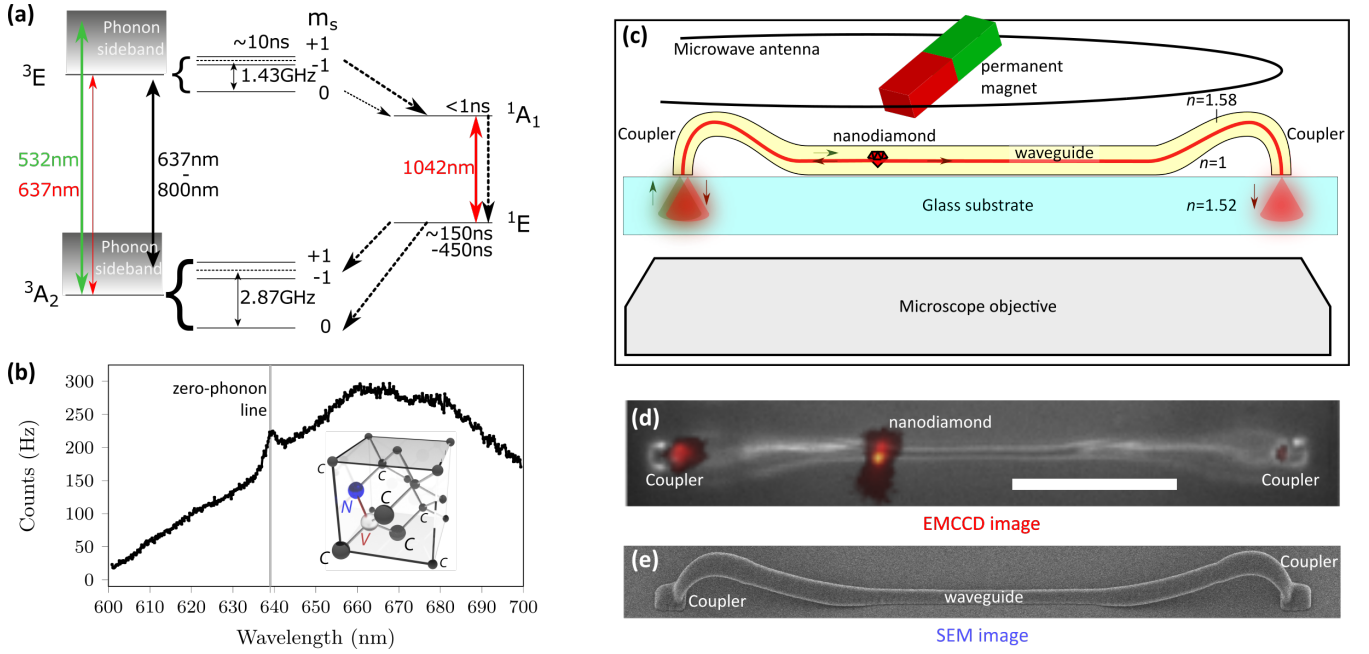


FIG. 1. (a) Level structure of the NV center [17–19], (b) fluorescence spectrum of the negatively charged NV center in the used nanodiamonds, inset: lattice structure of the NV center, the with the substitutional nitrogen atom in blue, the NV-axis in red and the vacancy in silver. (c) Sketch of the experimental setup. A green laser beam is coupled into the waveguide, containing a fluorescent nanodiamond. The fraction of the fluorescence guided in the waveguide is detected at the waveguide couplers, the unguided fraction is detected at the nanodiamond’s position. This is shown in the EMCCD image (d), where the reflected light microscope image is shown in gray scale, overlaid with the detected red fluorescent light from the nanodiamond. Scale bar: 20 μm . For comparison, a tilted SEM image of such a waveguide is shown in (e).

$$\hat{H} = D \left[\hat{S}_z^2 - \frac{S(S+1)}{3} \right] + \mu_B g_{\text{gs}}^{\parallel} \hat{S}_z \cdot B_z + \mu_B g_{\text{gs}}^{\perp} (\hat{S}_x B_x + \hat{S}_y B_y), \quad (1)$$

where D and $g_{\text{gs}}^{\parallel} = g_{\text{gs}}^{\perp} = g$ are the ground state splitting and the g -factor, respectively. Due to the system’s higher probability to undergo an intersystem crossing from the excited $m_s = \pm 1$ states to a long living singlet state, the system is optically pumped into the $m_s = 0$ ground state under optical excitation. This causes a higher fluorescence rate of the $m_s = 0$ state, harnessed in optical spin-state read-out.

In order to immerse nanodiamonds into the waveguides, we follow a probabilistic approach. The waveguides used are fabricated via direct laser writing in a polymer photoresist, using a commercial system (Nanoscribe Photonic Professional GT [21]). The nanodiamonds (120 nm size on average and more than 1200 NV centers per diamond) have been dispersed within the resist, see Appendix A. The waveguides feature bend radii down to 40 μm , insertion losses on the order of 10 dB, and show loss coefficients smaller than 0.81 dB/mm. To

insert and extract light to and from the waveguide, we use three-dimensional out of plane couplers, for details see Ref. [16]. In on average one out of eight written waveguides we find one and only one nanodiamond in the planar waveguide section, coupled to the waveguide modes. In FIG. 1(c-e), a sketch of the waveguide and its working principle are shown, as well as a light microscope image of a waveguide containing one single nanodiamond and an SEM image of a fabricated structure.

In order to excite integrated NV centers, a green laser beam ($\lambda = 532 \text{ nm}$) is focused onto the incoupling port of the waveguide, using a high numerical aperture objective (Nikon CFI Plan Apochromat Lambda 60XC). For fluorescence readout, an EMCCD-camera (Andor iXon 885) or a fiber-coupled single photon counting module (Laser-Components Count 100C-FC) is used.

As can be seen from FIG. 1(d), a nanodiamond excited by green light through the waveguide emits light both into free space and into the waveguide. An important question regards the coupling efficiency β of fluorescence light into the waveguide.

* landowski@physik.uni-kl.de

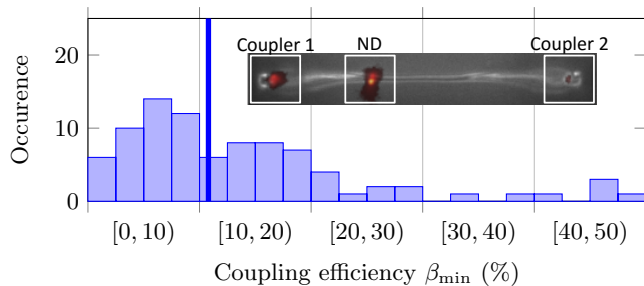


FIG. 2. Distribution of corrected coupling efficiencies of the total emission to one propagation direction. The excitation laser is coupled into the port named 'In', the fluorescence counts in the camera image are integrated over a small area surrounding the respective coupler or nanodiamond ('ND'). The median is marked in blue, negative values were neglected.

We define the minimum coupling efficiency

$$\beta_{\min} = \frac{\alpha}{\gamma} \cdot \frac{\mathcal{I}_{\text{coupler}}}{\mathcal{I}_{\text{ND}}}, \quad (2)$$

where $\mathcal{I}_{\text{coupler}}$ (\mathcal{I}_{ND}) is the fluorescence counts of the nanodiamond guided by the waveguide (emitted into free space) and simultaneously detected by an EMCCD camera; α corrects for the independently measured coupling loss of the waveguide coupler, and $\gamma = 9$ corrects for the limited numerical aperture of the imaging system collecting the free-space fluorescence for each coupler. We have verified that the fluorescence light originates from the nanodiamond rather than waveguide autofluorescence by modulating the fluorescence rate of the NV center via applying a microwave at the electronic spin resonance (ESR) at 2.865 GHz without an external magnetic field. Evaluating fifty nanodiamond-containing waveguides, we find a distribution of coupling efficiencies (see Fig. 2) with a median of $\beta_{\min} = (10.8 \pm 11.1)\%$, for details see Appendix C. From the comparison of free-space fluorescence and the fluorescence guided by the waveguide we also find that the ESR fluorescence contrast is only little affected by the waveguide, hence the contribution of waveguide fluorescence is negligible for the NV center concentration used.

III. MAGNETOMETRY

A possible limitation for application of NV centers as magnetometers is the need for direct optical access to the NV centers under investigation. We show that individual nanodiamonds carrying ensembles on NV centers integrated in our waveguides can be used for vector magnetometry, according to [22], where the waveguide is employed for guiding both excitation light as well as for the optical signal of the NV centers. Another possibility to extract the magnetic field components in a Cartesian basis is to modulate magnetic offset

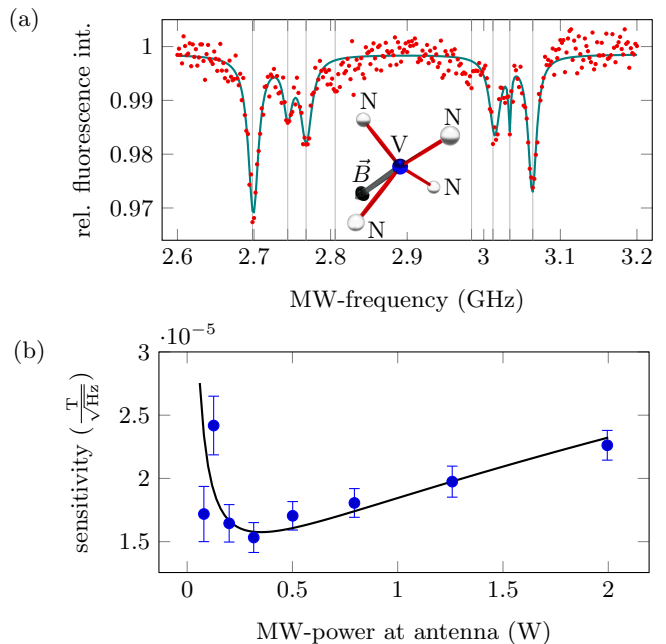


FIG. 3. (a) ODMR measurement on a nanodiamond detected *via* the waveguide. The inset shows the magnetic field orientation \vec{B} in grey, relative to the four NV center directions, retrieved from the fit data (a sum of six Lorentzians) shown as solid line. The magnetic field amplitude is measured to 16.1 mT from the ESR positions. (b) Calculated cw sensitivity of the NV centers used, depending on the applied MW-power. The solid curve is a fit to the data, given in the text.

fields in the respective directions with incommensurable frequencies, see [23].

To acquire fast ODMR spectra with high SNR, the microscope is used in confocal configuration, detecting the fluorescence power with a single photon counting module (SPCM). In the current setup, this is only possible for one spot under investigation at a given time. Such an ODMR spectrum measured *via* the waveguide is shown in FIG. 3. Further, the magnetic field orientation with respect to the diamond lattice is determined from this spectrum, see the inset in FIG. 3, and the magnetic field amplitude is determined to be 16.1 mT.

The figure of merit for a magnetometer is its sensitivity. For cw-ODMR measurements, the shot noise limited sensitivity is given by [24]

$$\eta_B = \mathcal{P} \frac{h}{g\mu_B} \frac{\Delta\nu}{C\sqrt{\mathcal{R}}} \quad (3)$$

where $\mathcal{P} \approx 0.77$ for a Lorentzian resonance shape, $\Delta\nu$ is the FWHM of the dip, C is the dip depth, and \mathcal{R} is the detected count rate. We determine the sensitivity of the waveguide-coupled magnetometer for a fixed laser power by measuring the width and depth of the dip at lowest frequency while varying the microwave power, see

FIG. 3. We fit the sensitivity with a function of the form $\eta_B = C \cdot \sqrt{a + \frac{P}{b} / (\frac{P}{P+a+b})}$, with $a = 0.1721$, $b = 0.03232$, $C = 46.3 \cdot 10^{-5}$, which is a simplified form of the theoretical description in [24] for constant excitation laser power. The minimum sensitivity is $(1.53 \pm 0.12) \times 10^{-5} \text{ T}/\sqrt{\text{Hz}}$ at a microwave power of 0.316 W applied to the wire loop antenna. For higher microwave powers, the width of the resonance is dominated by power broadening of the microwave, for lower powers power broadening of the resonance due to the laser polarizing the spin state dominates the sensitivity.

To circumvent power broadening, a pulsed measurement scheme, temporarily separating microwave and laser pulses can be used [24]. For the nanodiamonds we use, this is limited by the diamonds' quality.

IV. COHERENT SPIN DYNAMICS

A remarkable property of the NV center is its relatively long room-temperature spin-coherence time, which can reach $T_2 = 3 \text{ ms}$ [2], depending on the diamond's quality. It is known that for nanodiamonds, the surface can have profound impact on the embedded NV-centers' coherence times. Therefore we verify that integrating the nanodiamonds into the photoresist does not alter the NV centers' coherence time, which might be due to, *e.g.*, a modification of the nanodiamond surface due to the polymer matrix, potentially during direct-laser writing. We show the remote detection of Rabi nutations of an ensemble of NV centers through an optical waveguide, see FIG. 4, where the coherence time is compatible to the coherence time of uncoupled nanodiamonds, limited by the impurities in the volume and on the surface of the nanocrystals. Without waveguide, we measure typical coherence times of $T_2 = 1 \mu\text{s}$ and $T_2^* = 80 \text{ ns}$.

In order to address only one single spin transition of one NV orientation of the ensemble, an external magnetic field is applied and an ODMR spectrum recorded. A well separated ESR with dip depth of around 3% is chosen for the microwave frequency. The Rabi measurement sequence consists of three pulses. First, the spin ensemble is initialized in the $m_s = |0\rangle$ state *via* a green laser pulse of $50 \mu\text{s}$ duration, coupled to the waveguide. Second, the microwave pulse of varied length is applied transferring the addressed ensemble spins into the state $m_s = |-1\rangle$ or $|1\rangle$. Subsequently, a green laser pulse for state read-out is coupled to the waveguide, similar to initialization. The fluorescence light emitted during the first $1.5 \mu\text{s}$ of the readout pulse of $3 \mu\text{s}$ duration is guided to an SPCM *via* the waveguide and the confocal microscope. The detected number of photons is normalized to the number of photons detected without the microwave field applied, and it shows oscillation between the two spin states. The excitation pulses are chosen relatively long compared to single emitters to protect the SPCM from to intense illumination due to the large NV ensembles investigated.

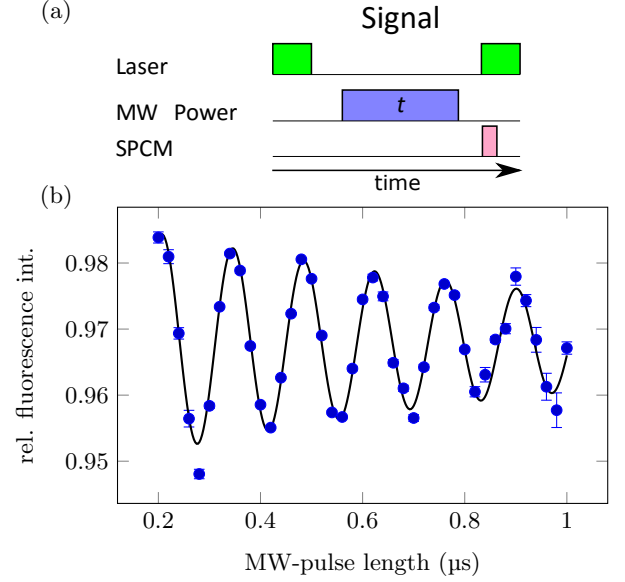


FIG. 4. (a) Experimental sequence to measure Rabi nutations, (b) Rabi oscillations of NV centers in a single nanodiamond, detected via the waveguide. 2 W MW power at the antenna. The solid line is a fit to a damped sine, yielding a damping time of $T \approx 1 \mu\text{s}$.

In order to remove effects from drifts, or fluctuations of, *e.g.* surface charges and charge states of crystal defects, this sequence is followed by the same sequence without microwave pulse, which is used as reference for normalization.

The Rabi oscillations detected show a coherence time of $1 \mu\text{s}$, which is comparable to coherence times measured in bare nanodiamonds. We expect that reducing the number of surface impurities and lowering the N-concentration of the nanodiamonds embedded into the waveguides will enhance coherence times [25, 26].

V. CONCLUSION

We have shown the integration of single crystalline nanodiamonds containing an ensemble of NV centers into direct-laser-written waveguides, which enable the creation of extended three-dimensional waveguide networks on a chip. These NV centers can be used as integrated sensors for magnetic fields, which are initialized and read out via the waveguides they are embedded in.

The ODMR signal of the NV ensemble is not affected by fluorescence of the waveguide material. However for small ensembles or even single NV centers the fluorescence contributions of different origin might be separated by harnessing the strongly different lifetimes of 33.6 ns (5.28 ns) for NV centers (photoresist), see Appendix B. Further, we have shown the detection of rabi oscillations *via* the waveguide housing the nanodiamond, allowing

for coherent control over an ensemble of remote quantum emitters. The T_2^* time of the NV ensembles is relatively short ($T_2^* \approx 80$ ns), probably limited by the large number of impurities in our nanodiamonds and on its surface. While this prevents their use for magnetometry using a Ramsey scheme, this limitation can be overcome by employing nanodiamonds with improved coherence properties. Thereby, our waveguides pave the way to optical networks, hosting three-dimensional arrays of spin sensors. In the future it will be interesting to explore the prospects of three-dimensional sensors detecting magnetic fields as well as gradients in a small volume by direct-laser-written three-dimensional photonic structures with multiple nanodiamonds embedded. These sensors are also useful for sensitive or biological samples under investigation, since the laser light used to read out the NV centers is guided within the waveguide, reduc-

ing the amount of optical power deposited at the sample by orders of magnitude and simultaneously keeping the whole sample optically accessible. At the same time, the processed photoresist is stable against watery solutions and might thus be compatible with sensing applications in life science.

ACKNOWLEDGMENTS

We thank Henning Fouckhardt and his group Integrierte Optoelektronik und Mikrooptik (Technische Universität Kaiserslautern) for access to their wet chemistry lab, and we also acknowledge the technical support by the Nano Structuring Center (Technische Universität Kaiserslautern). Furthermore, we thank Stefan Dix for help with the experimental setup.

-
- [1] F. Jelezko, T. Gaebel, I. Popa, A. Gruber, and J. Wrachtrup, Physical review letters **92**, 076401 (2004).
 - [2] N. Bar-Gill, L. M. Pham, A. Jarmola, D. Budker, and R. L. Walsworth, Nature communications **4**, 1743 (2013).
 - [3] G. Balasubramanian, I. Y. Chan, R. Kolesov, M. Al-Hmoud, J. Tisler, C. Shin, C. Kim, A. Wojcik, P. R. Hemmer, A. Krueger, T. Hanke, A. Leitenstorfer, R. Bratschkitsch, F. Jelezko, and J. Wrachtrup, Nature **455**, 648 (2008).
 - [4] J. R. Maze, P. L. Stanwix, J. S. Hodges, S. Hong, J. M. Taylor, P. Cappellaro, L. Jiang, M. V. G. Dutt, E. Togan, A. S. Zibrov, A. Yacoby, R. L. Walsworth, and M. D. Lukin, Nature **455**, 644 (2008).
 - [5] M. S. Grinolds, S. Hong, P. Maletinsky, L. Luan, M. D. Lukin, R. L. Walsworth, and A. Yacoby, Nature Physics **9**, 215 (2013).
 - [6] A. O. Sushkov, I. Lovchinsky, N. Chisholm, R. L. Walsworth, H. Park, and M. D. Lukin, Physical Review Letters **113**, 197601 (2014).
 - [7] G. Kucsko, P. C. Maurer, N. Y. Yao, M. Kubo, H. J. Noh, P. K. Lo, H. Park, and M. D. Lukin, Nature **500**, 54 (2013).
 - [8] B. Hensen, H. Bernien, A. E. Dréau, A. Reiserer, N. Kalb, M. S. Blok, J. Ruitenber, R. F. L. Vermeulen, R. N. Schouten, C. Abellán, W. Amaya, V. Pruneri, M. W. Mitchell, M. Markham, D. J. Twitchen, D. Elkouss, S. Wehner, T. H. Taminiau, and R. Hanson, Nature **526**, 682 (2015).
 - [9] T. M. Babinec, B. J. M. Hausmann, M. Khan, Y. Zhang, J. R. Maze, P. R. Hemmer, and M. Lončar, Nature Nanotechnology **5**, 195 (2010).
 - [10] P. Maletinsky, S. Hong, M. S. Grinolds, B. Hausmann, M. D. Lukin, R. L. Walsworth, M. Loncar, and A. Yacoby, Nature Nanotechnology **7**, 320 (2012).
 - [11] S. A. Momenzadeh, R. J. Stöhr, F. F. de Oliveira, A. Brunner, A. Denisenko, S. Yang, F. Reinhard, and J. Wrachtrup, Nano letters **15**, 165 (2015).
 - [12] S. L. Mouradian, T. Schröder, C. B. Poitras, L. Li, J. Goldstein, E. H. Chen, M. Walsh, J. Cardenas, M. L. Markham, D. J. Twitchen, M. Lipson, and D. Englund, Physical Review X **5** (2015), 10.1103/PhysRevX.5.031009.
 - [13] A. W. Schell, J. Kaschke, J. Fischer, R. Henze, J. Wolters, M. Wegener, and O. Benson, Scientific reports **3**, 1577 (2013).
 - [14] Q. Shi, B. Sontheimer, N. Nikolay, A. W. Schell, J. Fischer, A. Naber, O. Benson, and M. Wegener, Scientific reports **6**, 31135 (2016).
 - [15] J. P. Hadden, V. Bharadwaj, B. Sotillo, S. Rampini, R. Osellame, J. D. Witmer, H. Jayakumar, T. T. Fernandez, A. Chiappini, C. Armellini, M. Ferrari, R. Ramponi, P. E. Barclay, and S. M. Eaton, Optics letters **43**, 3586 (2018).
 - [16] A. Landowski, D. Zepp, S. Wingerter, G. von Freymann, and A. Widera, APL Photonics **2**, 106102 (2017).
 - [17] K. Jensen, N. Leefer, A. Jarmola, Y. Dumeige, V. M. Acosta, P. Kehayias, B. Patton, and D. Budker, Physical review letters **112**, 160802 (2014).
 - [18] V. M. Acosta, A. Jarmola, E. Bauch, and D. Budker, Physical Review B **82** (2010), 10.1103/PhysRevB.82.201202.
 - [19] L. J. Rogers, M. W. Doherty, M. S. J. Barson, S. Onoda, T. Ohshima, and N. B. Manson, New Journal of Physics **17**, 013048 (2015).
 - [20] M. W. Doherty, N. B. Manson, P. Delaney, F. Jelezko, J. Wrachtrup, and L. C. Hollenberg, Physics Reports **528**, 1 (2013).
 - [21] Nanoscribe GmbH, *Photonic Professional (GT): User Manual* (2017).
 - [22] S. Kitazawa, Y. Matsuzaki, S. Saijo, K. Kakuyanagi, S. Saito, and J. Ishi-Hayase, Physical Review A **96** (2017), 10.1103/PhysRevA.96.042115.
 - [23] J. M. Schloss, J. F. Barry, M. J. Turner, and R. L. Walsworth, Physical Review Applied **10** (2018), 10.1103/PhysRevApplied.10.034044.
 - [24] A. Dréau, M. Lesik, L. Rondin, P. Spinicelli, O. Arcizet, J.-F. Roch, and V. Jacques, Physical Review B **84** (2011), 10.1103/PhysRevB.84.195204.
 - [25] J. Tisler, G. Balasubramanian, B. Naydenov, R. Kolesov, B. Grotz, R. Reuter, J.-P. Boudou, P. A. Curmi, M. Senour, A. Thorel, M. Börsch, K. Aulenbacher, R. Erdmann, P. R. Hemmer, F. Jelezko, and J. Wrachtrup,

ACS nano **3**, 1959 (2009).

[26] H. S. Knowles, D. M. Kara, and M. Atatüre, Nature materials **13**, 21 (2014).

[27] Comsol, “Comsol wave optics module,”.

Appendix A: Nanodiamond integration into photoresist

Nanodiamonds containing NV ensembles are immersed into the photoresist EpoClad 50 (Microresist). The nanodiamonds (sigma aldrich, '798088') are suspended in deionized water in a concentration of 1 mg/ml and are used as received. Their size is 120 nm on average and they contain more than 1200 NV centers, each. For the integration into EpoClad, the deionized water is exchanged by the solvent of EpoClad, gammabutyrolactone (GBL). This is achieved by, first, centrifugating the suspension for 15 min at 6000 rpm, and second, exchanging the water by the same amount of GBL. To suspend the new mixture, it is vortexed and exposed to an ultra sonic bath to disperse agglomerates into single crystalline nanodiamonds. This procedure is repeated two times to ensure a low residual water concentration. Equal mass ratios of the suspension and EpoClad 50 are mixed for 30 min at 200 rpm, using a magnetic stir bar. The photoresist with immersed nanodiamonds is processed for direct laser writing as described in Ref. [16].

Appendix B: Waveguide influence on optical nanodiamond signal

In order to compare the ODMR signal collected directly from the nanodiamond at the one hand and via the waveguide at the other hand, an ODMR measurement is taken. Using the microscope's EMCCD camera both the waveguide port and the nanodiamond's free-space fluorescence are imaged simultaneously. The resulting spectra are shown in FIG. 5, showing an almost identical signal. Particularly, this shows that the waveguide does not add noise to the signal, which might stem from, *e.g.*, parasitic fluorescence. The ODMR measurement taken with direct excitation at the nanodiamond may differ in the contrast of specific dips, which is a polarization effect, but not in their positions.

In the case presented here, on the order of 10^3 nanodiamonds contribute to the signal. Neglecting the influence of the polymer waveguide might thus not be valid for weaker signals of few or single NV centers. In this case, the contribution of NV fluorescence versus waveguide fluorescence may still be separated by exploiting markedly different time scales of fluorescence lifetimes in a pulsed measurement, as shown in Fig. 6.

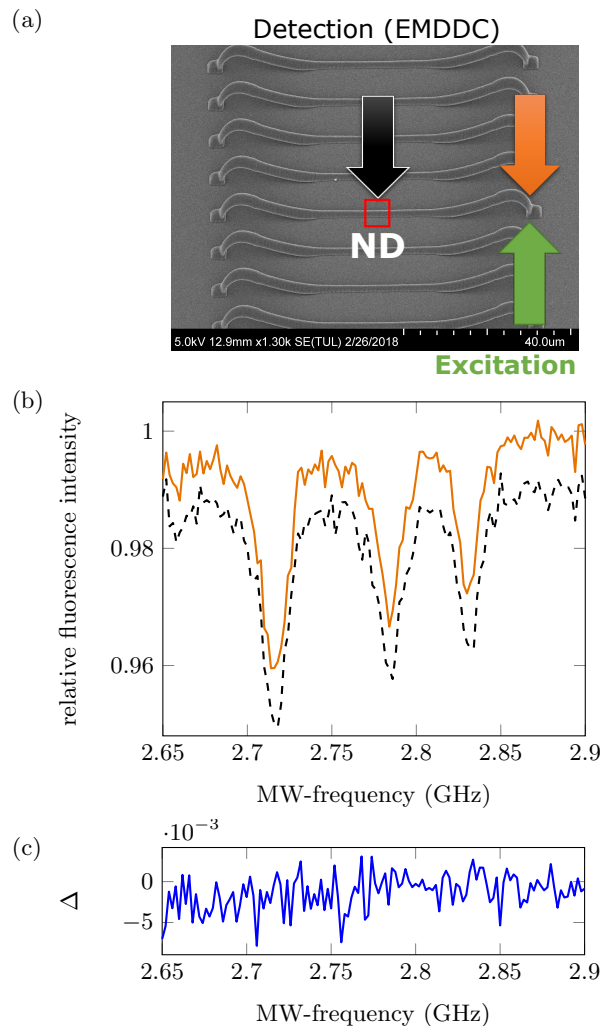


FIG. 5. (a) SEM image of series of direct-laser-written waveguides with nanodiamond indicated by square. (b) Comparison of ODMR signals excited via the waveguide and detected via waveguide (orange), free space (dashed black, shifted vertically by -0.01). (c) Shows the difference Δ of both signals.

Appendix C: Coupling efficiency

Experimentally, we determine the quantities in Eq. (2) to extract the minimum coupling efficiency β_{\min} . Evaluating camera images, we can simultaneously determine the fluorescence of the nanodiamond emitted into free space $\mathcal{I}_{\text{coupler}}$ and the guided fluorescence at the waveguide output couplers \mathcal{I}_{ND} . The free-space emission is corrected for finite detection solid angle by parameter β . Assuming an isotropic nanodiamond emission, the geometry of the setup yields a collection efficiency of 11 % at the nanodiamond position using a microscope objective with $\text{NA} = 0.95$. The waveguide coupling losses have been measured in Ref. [16]. We correct for these losses by the factor α .

We prepare and measure 50 nanodiamonds, each em-

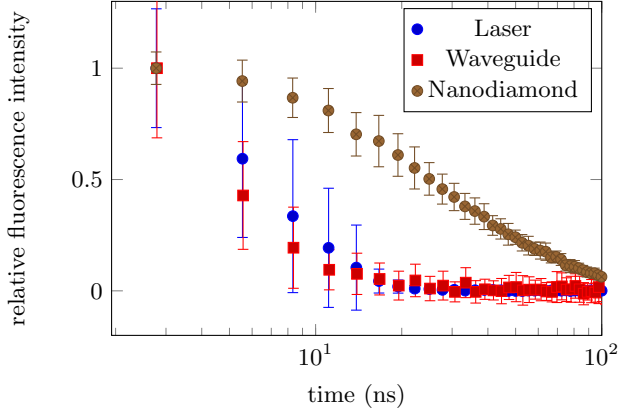


FIG. 6. Fluorescence lifetimes of the photoresist measured by exciting a waveguide in comparison to lifetime of NV centers in nanodiamond and the laser switching characteristics. The fluorescence signal of the resist is much noisier due to the low countrate (ratio of initial countrates is approximately 10^2), the fluorescence intensity of each data set is independently normalized to 1 in the beginning. The errorbars are statistical (1σ) errors.

bedded in another waveguide structure. In order to separate NV center signal from other unwanted signals, we record ODMR spectra. Before extracting the coupling efficiency reported in Fig. 2, we investigate if the polymer waveguide influences the ODMR signal itself. To this end, we compare the relative fluorescence counts of an ODMR signal at a microwave frequency of 2.865 GHz (vertical line in the inset of Fig. 2), where the signal is either guided in the waveguide (yielding contrast C_i for counts in coupler i) or detected from free-space radiation (contrast C_{ND}). The distribution of ratios between both contrasts is shown in Fig. 7 and it is well centered around unity (median of 0.978).

Comparing the ODMR-signal counts at the waveguide couplers with those detected from free space, we get a median bare ratio of the counts of $\mathcal{I}_{\text{coupler}}/\mathcal{I}_{ND} = (3.8 \pm 3.9)\%$ for the coupling efficiency of total emission to the waveguide modes propagating into one direction, with error given by standard deviation, see FIG. 2. If we take the independently measured coupling loss of 4.5 dB [16] into account, the coupling efficiency is multiplied by a factor of 2.85, yielding a corrected median coupling efficiency of $\beta_{\min} = (10.8 \pm 11.1)\%$.

We conclude that for our concentration of NV centers in the nanodiamond the fluorescence contrast is only little affected by the waveguide, which shows that the contribution of waveguide fluorescence is negligible for the NV center concentration used.

Additionally, simulations in Comsol Wave Optics [27] have been performed, see Fig. 8. From the simulation, the maximum coupling efficiency of the integrated emitters to the waveguide mode, i.e. the β -factor, is retrieved to be $\beta_{\max} = 12.2\%$ for one propagation direction. This

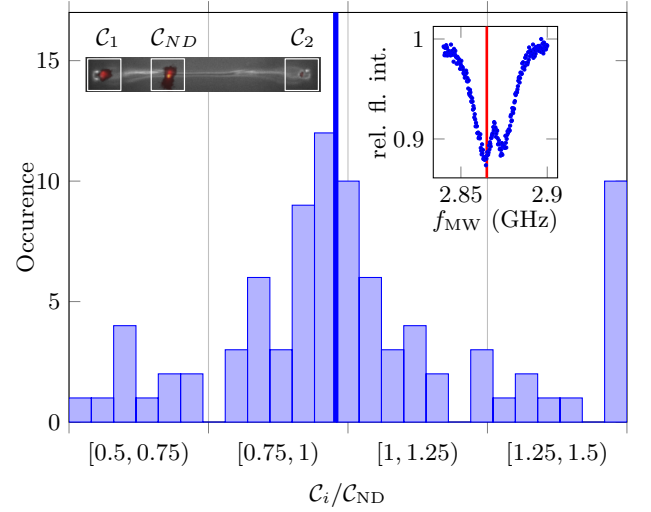


FIG. 7. Distribution of ratio of ESR contrasts C_i at 2.865 GHz, detected at the couplers $i = 1, 2$ relative to the contrast C_{ND} , detected at the nanodiamond. The median is marked in blue. The contrast C_i is defined as $C_i = 1 - \frac{\mathcal{I}'_i}{\mathcal{I}_i}$, where \mathcal{I}'_i (\mathcal{I}_i) is the detected count rate at position i with (without) microwave applied. (insets) Free space ODMR spectrum in absence of an external magnetic field, the microwave frequency used is marked in red; microscope image of a waveguide under investigation with marked positions for evaluation.

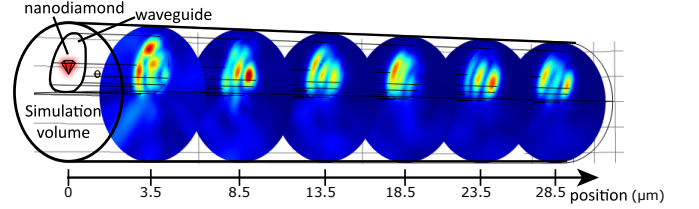


FIG. 8. Simulated propagating light field in the wave guide, emitted by a nanodiamond positioned at the center of the fundamental mode. From the ratio of guided energy to total irradiated energy the coupling factor can be deduced.

value, however, does not include any experimental imperfections, such as finite solid detection angle or coupling and propagation loss of the waveguides. From a planar diamond membrane, only approximately 8% of the emitted photons would be collected by a standard microscope objective with NA=1.3.